Green synthesized nano-scale iron for oxidative catalysis of organic environmental pollutants

ARTICLE · JANUARY 2014

1 AUTHOR:

Homer Genuino
Utrecht University
42 PUBLICATIONS **448** CITATIONS

CHAPTER

3

Green Synthesis of Iron Nanomaterials for Oxidative Catalysis of Organic Environmental Pollutants

Homer C. Genuino[a], *Nashaat Mazrui*[a], *Mohammad S. Seraji*[a], *Zhu Luo*[a], *and George E. Hoag*[b]

[a]**Department of Chemistry, University of Connecticut, 55 North Eagleville Road, Storrs, CT 06269-3060, USA**

[b]**VeruTEK Technologies, Inc., 65 West Dudley Town Road, Suite 100, Bloomfield, CT 06002, USA**

3.1 SYNTHESIS

Iron nanomaterials have been extensively used in different fields including food-related applications [8], medical uses [65], biosensing applications [31], and degradation of environmental organic contaminants [60,73]. These important applications are achievable due to versatile properties and high catalytic activities of iron nanomaterials. Most notably, iron nanomaterials are widely used in environmental remediation. Common examples of iron nanomaterials utilized in this area include zero-valent iron, iron oxides, iron phosphate, and iron-based bimetallic particles. Green-synthesized iron nanomaterials can also be obtained using plant extracts and microorganisms.

The majority of nanomaterials are synthesized via two common approaches—the top-down method and the bottom-up method (Figure 3.1) [28]. In the top-down method, nanosized materials are generated from breaking down of bulk materials, whereas in the bottom-up method, atoms and molecules assemble to form nanosized structures. Based on these two approaches, different synthesis methods of nanoparticles have been established including

http://dx.doi.org/10.1016/B978-0-444-53870-3.00003-4

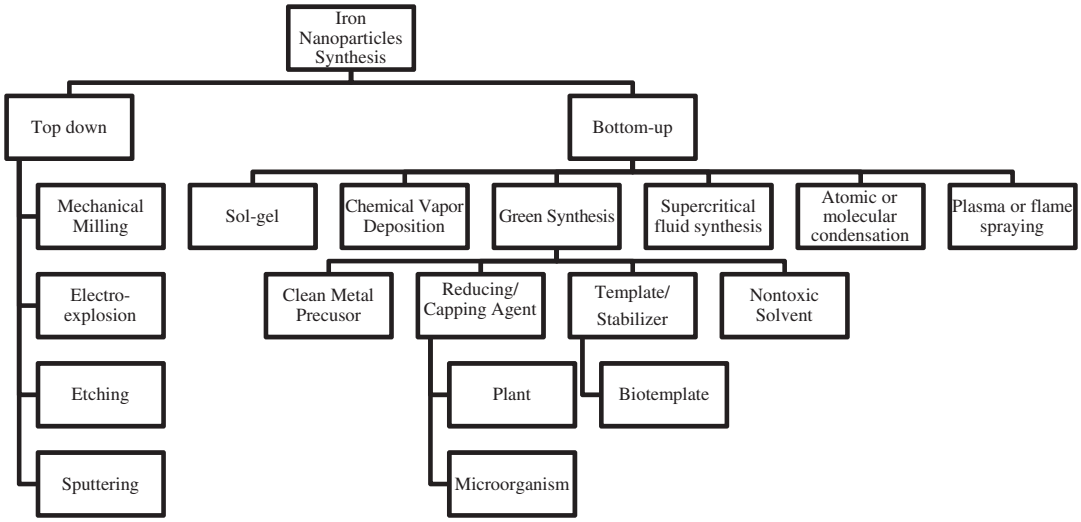

FIGURE 3.1 Various methods for the synthesis of iron-containing nanoparticles.

chemical, physical, and biological pathways [14]. However, current chemical and physical methods for the synthesis of iron nanoparticles involve some inevitable drawbacks including high energy cost, environmental pollution, and production of toxic by-products [5]. In particular, the reducing agents, capping agents, templates, and solvents used are considered hazardous, posing significant environmental and biological risks [44]. Alternatively, green synthesis methods of metal nanoparticles have recently been studied to produce novel nanomaterials which are environmental friendly, safe to humans, and sustainable for commercial use [3]. Green chemistry principles can be incorporated into the synthesis of nanoparticles by considering the proper choice of reducing agents, capping agents, solvents, supports, and methods for surface modification. The methods used to synthesize these iron-containing materials are reviewed in the following sections.

3.1.1 Zero-Valent Iron (ZVI)

ZVI has been used as an effective material to remediate large quantities of organic contaminants in the environment due to its magnetic and catalytic properties, low toxicity, and relatively low cost [1,12,16,32,34]. ZVI has also been regarded as a green material due to large amount of iron available as recycled material and its ability to completely degrade some contaminants [34]. One notable advantage of using nZVI is its small size, which allows the particles to suspend in water for a longer time, making nZVI useful for *in situ* treatment of contaminated water [59]. The traditional method used for the synthesis of nZVI is the reduction of ferrous or ferric ion using borohydride in aqueous solution, as shown in Eqs. (3.1) and (3.2) [2,11,41,63].

$$2Fe^{2+}(aq) + BH_4^-(aq) + 3H_2O(l) \rightarrow 2Fe^0(s) + H_2BO_3^-(aq) + 4H^+(aq) + 2H_2(g) \quad (3.1)$$

$$4Fe^{3+}(aq) + 3BH_4^-(aq) + 9H_2O(l) \rightarrow 4Fe^0(s) + 3H_2BO_3^-(aq) + 12H^+(aq) + 6H_2(g) \quad (3.2)$$

Another method is through the thermal decomposition of iron pentacarbonyl ($Fe(CO)_5$) in organic solvents or in argon. Although popular, these methods have some disadvantages, which include (1) removal of the by-product from the reduction process such as the removal of borate and stoichiometric excess borohydride; (2) high cost of toxic reagents such as $Fe(CO)_5$; and (3) production of a large amount of wastewater during preparation [34].

3.1.2 Iron Oxide

The most common iron oxide nanoparticles utilized for water remediation are magnetite (Fe_3O_4) [5], hematite (Fe_2O_3) [13], maghemite (γ-Fe_2O_3) [7], goethite, and ferrihydrite [22]. Iron oxide nanoparticles have attracted attention due to their excellent chemical stability, high catalytic activity [52], and low toxicity [23]. Oxides of iron also have distinct magnetic properties. Current chemical methods for the synthesis of iron oxides nanoparticles include sol-gel, forced hydrolysis, sonochemical, and electrochemical methods [7]. However, these methods generally require a great deal of energy and produce particles in non-polar organic solutions [7].

3.1.3 Iron Phosphate

Iron phosphate nanoparticles have excellent physical and chemical properties, high reactivity, are relatively inexpensive to synthesize, and are biocompatible. They have been extensively applied to catalytic reaction, environment purification, ferroelectrics [4], and lithium ion batteries. The different types of iron phosphate are delithiated LiFePO [10], monoclinic $FePO_4$, orthorhombic $FePO_4$ hydrated phases, which include phosphosiderite (or metastrengite) $FePO_4{\cdot}2H_2O$ monoclinic and $FePO_4$ $2H_2O$ orthorhombic forms [71]. These materials are obtained based on various types of preparation methods such as sol-gel [29–31], ion-exchange [39], co-precipitation [69], and microwave-assisted synthesis [70]. The main disadvantages of these methods are low production yield and complicated synthesis steps.

3.1.4 Iron Bimetallic

The catalytic activity of iron nanoparticles for application such as dechlorination process in wastewater treatment may decrease over time due to the decrease in the number of surface active sites [45]. In order to prevent blocking of these active sites, a second metal is frequently added [68]. Various iron bimetallic systems have been reported in the literature including Fe/Pt, Fe/Ag, Fe/Cu [76], Fe/Ni [64], and Fe/Pd [35]. Iron can generate H_2 gas during the corrosion reaction in water and the second metal acts as a hydrogenation catalyst [61]. Enhanced dehalogenation by iron nanoparticles coated with Pd has also been reported [74]. Green synthesis of these bimetallic nanoparticles is feasible. For instance, He and Zhao used starch to stabilize the iron nanoparticles, overwhelming the difficulty of particle agglomeration and achieving high catalytic activity for dechlorination process [24]. Moreover, Smuleac et al. successfully synthesized Fe/Pd nanoparticles using green tea extract as a reducing agent instead of using $NaBH_4$ [61].

3.1.5 Green Reducing Agents

The green synthesis method utilizing plant extracts or microorganisms has been used as an environmental-friendly approach for the synthesis of metallic nanoparticles. Plant extracts and microorganisms can act as reducing agents in replacement of toxic reductants such as borohydride. Particularly, plant extracts are capable of reducing a variety of iron salts to generate nZVI. Successful synthesis of iron nanoparticles utilizing tea leaf [43], alfafa biomass [26], sorghum bran extracts [48], and fungi [5] has been reported recently. The synthesis of iron nanoparticles using extracts from biological sources is significantly easier as compared to conventional chemical methods. For example, plant iron salt solutions can simply be added to the plant extract solution with an optimum volume ratio at ambient temperatures and pressures. The utilization of natural or organic acids is also an alternative way for iron nanoparticle preparation. Herrera-Becerra et al. used tannic acid and gallic acid as reducing agents to prepare iron oxide nanoparticles [25]. On the other hand, Meeks et al. successfully used ascorbic acid for the synthesis of iron-based nanoparticles [41]. Another important route to prepare iron nanomaterials is the use of microorganisms such as bacteria, fungi, and yeast. In the 1980s and 1990s, scientists had already conducted research on iron-reducing microorganisms [15,38]. Recently, Bharde et al. reported that nanocrystalline magnetite is formed within 24 h by reaction of *Actinobacter* spp. with an aqueous potassium ferricyanide/ferrocyanide mixture under fully aerobic conditions [6]. These microbes yield inorganic materials often having a fine morphology either through intracellular or extracellular mechanisms. Based on reducing or precipitating soluble toxic metal ions, microorganisms generate insoluble nontoxic metal nanoclusters [47]. The advantages of green reducing agents are that they are environmentally benign and the products obtained are both stable and controllable. When using a strong reducing agent (e.g., $NaBH_4$), the initially generated nanoparticles may react with dissolved oxygen and water, as shown in Eqs. (3.3) and (3.4).

$$2Fe^0(s) + 4H^+(aq) + O_2(g) \rightarrow 2Fe^{2+}(aq) + 2H_2O(l) \tag{3.3}$$

$$Fe^0(s) + 2H_2O(l) \rightarrow Fe^{2+}(aq) + H_2(g) + 2OH^-(aq) \tag{3.4}$$

Additionally, the agglomeration may become faster, leading to the loss of reactivity of nanoparticles [24].

3.1.6 Green Capping Agents

Capping agents are crucial for the formation of nanoparticles because they can affect the growth mechanism of nanoparticles by sorption on the growing face of nanoparticles. Capping agents can also adjust the size and morphology of nanoparticles by varying the quantity of capping agent [56]. Therefore, the synthesis of nanomaterials with capping agents becomes controllable and produces stable nanoparticles that are less susceptible to agglomeration and chemical alteration reactions. Synthesis of nanomaterials using chemical capping agents such as ethylenediaminetetraacetic acid, triethanolamine [58], and tetraethylammonium bromide [9] has been previously studied. However, many of the common chemical capping agents are known to bioaccumulate in the environment and are persistent pollutants,

which may have ecological or human health risks. During the process of green synthesis, environmental-friendly capping agents are applied in the system instead of chemical capping agents. For example, sorghum bran extract and tea polyphenols [55] have been reported to be effective for controlling iron nanoparticle size during synthesis. Additionally, they simultaneously act as reducing agents. The plant extracts are easy to obtain—usually a certain amount of extract is stirred and heated in water at temperatures slightly <100 °C. After a short settling time, the extract is vacuum-filtered and then the solution is ready to use.

3.1.7 Green Template/Surfactant

Frequently, templates or surfactants are required for nanoparticle synthesis in order to control the growth of nanoparticles and prevent aggregation. Templates or surfactants limit nanoparticle size by the void spaces of porous structure, managing the size of micelles [50]. Using a template, synthesis tends to only react with target reactants, aggregation can be prevented, and hierarchically architectured materials can be obtained [37]. Biotemplates have been successfully utilized with green synthesis systems of iron nanoparticles in an environmentally benign way. Green templates from plant extracts have been described in a number of studies, and they are typically added to the solution with appropriate amount of iron salts and stirred for a certain period of time to achieve equilibrium. Plant-based surfactants such as VeruSOL-3, VeruSOL-10, VeruSOL-11, and VeruSOL-12 can even work without any special reducing agents or capping agents for the preparation of nanostructures [44]. Moreover, microorganisms can create a well-dispersed nanoparticle system with a multitude of nucleation centers [66]. Zhou et al. utilized yeast cells as a biotemplate to provide nucleation sites for induced growth of iron nanoparticles [75]. Even viruses such as the *Cowpea mosaic* virus have been reported as templates for directing the formation of monodisperse, hollow structure iron-platinum nanoparticles [54].

3.1.8 Green Solvents

Co-precipitation and decomposition of salts in high boiling organic solvents are effective approaches to obtain iron oxide nanomaterials for large-scale production and enhanced magnetic properties. However, not all solvents used for synthesis are benign. Srivastava et al. presented an innovative method and successfully prepared citrate-coated Fe_3O_4 nanoparticles using nonhazardous iron salts and a biodegradable capping agent [62]. Park et al. also investigated the use of green solvents for the synthesis of iron nanoparticles [49]. In their work, ionic liquids-based green nanotechnology was utilized to control the size of iron nanoparticles using neoteric solvents. Ionic liquids-based green solvents can be used both as a templating and as a co-solvent agent during synthesis.

3.2 CHARACTERIZATION

An understanding of the physical and chemical properties of nanomaterials is the key for their proper application. Iron nanomaterials such as zero-valent iron, iron oxides, and iron bimetallics have been synthesized by different methods and in different forms. A review of

some of their properties such as structure, morphology, textural properties, and composition is given in the following sections.

3.2.1 Structures

The structure of nanomaterials can be elucidated using various techniques including X-ray diffraction (XRD), X-ray absorption near-edge structure spectroscopy (XANES), Raman spectroscopy, X-ray photoelectron spectroscopy (XPS), and Fourier-transform infrared (FTIR) spectroscopy. For example, XRD analysis of green-synthesized iron nanomaterials from green tea leaf extracts was carried out using a Philips X'Pert Pro instrument with the source of Cu Kα radiation ($\lambda = 1.54$ Å) and the samples were scanned within 20–70° (2θ value) [55]. The nanomaterials were repeatedly washed with ethanol prior to XRD analysis. XRD patterns corresponded to iron oxide and iron oxohydroxide. FTIR spectra of these iron nanoparticles were obtained by direct analysis using Varian Carry 50 spectrophotometer. Several peaks in the spectral range 800–1800 cm^{-1} were attributed to the polyphenols that were presumably present at the surface of iron nanoparticles. A very strong peak at 1065 cm^{-1} was attributed to the stretching vibration of C–O–C. A peak at 1400 cm^{-1} corresponded to the in-plane bending vibration of –OH in phenol and a peak at around 1600 cm^{-1} was attributed to the C═C ring stretching in polyphenols.

In a separate study, the XRD patterns of iron nanoparticles were identified as the face-centered cubic spinel structure of pure Fe_3O_4 with a lattice parameter of $a = 8.393$ Å, which was very close to the reported value (JCPDS 65-3107) [77]. However, the XRD patterns of iron nanoparticles from sorghum bran extracts did not show the distinct diffraction peaks, suggesting a possible formation of amorphous structure of the prepared iron nanomaterials [48]. Single-step green synthesis of iron nanomaterials from tea polyphenols was also conducted. The XRD pattern of the iron nanoparticles was compared with JCPDS pattern 00-050-1275 and found that the highest intensity plane (1 0 2) was in line with the reported pattern [27].

In another study, broad peaks in the XRD patterns were obtained, which also revealed the existence of an amorphous phase of iron [78]. Other apparent peaks were present at $2\theta = 44.9°$ and 35.8°, which strongly indicated the presence of both zero-valent iron as α-Fe and iron oxide crystalline phase. These structures were further confirmed using XPS technique (Yuan-Pang et al.). XANES results suggested that about 44% of the nanoparticles were composed of zero-valent iron and the remaining as FeO [78]. Contrary to what others observed, the sample did not contain Fe^{3+}. The ensemble of XRD, XPS, and XANES results concluded that the nanoparticles were likely to have a core of zero-valent iron, whereas the shell was largely made of iron (II) oxide [78].

Paramagnetic iron oxide nanoparticles were synthesized in the presence of polymerized lactic acid [79]. The XRD pattern of the magnetic nanoparticles (Fe_3O_4 crystals) showed the inverse cubic spinal structure having six diffraction peaks consistent with the standard pattern at (2 2 0), (3 1 1), (4 0 0), (4 2 2), (5 1 1), and (4 4 0) [79]. In addition, two FTIR peaks at 3400 cm^{-1} and 1622 cm^{-1} indicated the presence of carboxyl and hydroxyl groups, presumably on the polymer chain. Magnetic iron oxide nanomaterials were also prepared in a water-in-oil microemulsion system [80]. The well-defined XRD patterns indicated the crystalline structure of γ-Fe_2O_3 or magnetite; however, the peaks were quite broad indicating very small crystallite size.

The structure of coated iron nanoparticles cannot be determined by XRD alone. In the XRD pattern of Au-coated iron particles, all the reflections corresponded to the FCC bulk structure of gold, whereas the XRD patterns for α-iron were hidden under the XRD patterns of gold. This was found to be due to the overlap of their diffraction peaks ($2\theta = 44.8°$, 65.3°, and 82.5°) [81]. The energy-dispersive X-ray spectroscopy (EDXS) data indicated the presence of both iron and gold in the sample. High-resolution transmission electron microscopy (HRTEM) images revealed the interplanar distances about 2.0 Å and about 1.4 Å in the crystal lattice of iron core, which corresponded to the (1 1 0) and (2 0 0) lattice planes of iron [81].

Metallic iron nanoparticles are synthesized by reduction of goethite (Fe^{H2}) and reductive precipitation with borohydride (Fe^{BH}) [82]. The XRD patterns of Fe^{H2} showed two phases—α-Fe^0 and Fe_3O_4 (70–30% metal and 30–70% oxide, respectively). The mean crystalline dimension of α-Fe^0 was about 30 nm, whereas the Fe_3O_4 material was about 60 nm. However, the Fe^{BH} showed very broad peaks for α-Fe^0 with average crystalline dimensions <1.5 nm.

3.2.2 Morphology

TEM and field-emission scanning election microscopy (FESEM) are extremely useful techniques for morphology characterization of materials. The SEM images of green-synthesized iron nanomaterials were obtained using a Philips XL-350 FEG-type instrument [55]. From the TEM images obtained using a JEOL JEM 1200 EX Mk 2 TEM at 120 keV, particle size ranges from 40 nm to 60 nm were found, including those that formed and displayed some irregular clusters and dispersion.

In separate study, FESEM and TEM images of prepared nanoparticles were found to have a uniform and spherical morphology with an average diameter of about 27.2 nm [77]. The amorphous structure of iron nanomaterials prepared by Njagi et al. was viewed under FESEM. Images showed that the particles agglomerated to form irregular clusters. The selected area electron diffraction (SAED) micrographs had some diffuse ring instead of diffraction ring or spot further confirming the amorphous nature of the iron nanoparticles. The particles were also found to have an average diameter of about 50 nm, as shown in the TEM images in Figure 3.2 [48]. The sizes of the iron nanoparticles synthesized from green tea extract were found to vary from 5 nm to 15 nm [27]. The TEM images of these nanoparticles are likewise shown in Figure 3.3. The image also represents the spherical shape of the nanoparticles.

Apart from the green synthesis, some methods describe the preparation of zero-valent iron nanoparticles from the reduction of Fe(III) by sodium borohydride. Zero-valent iron nanoparticles prepared by Sun et al. were largely spherical with a particle size in the 60–70 nm range and the TEM images showed that most particles formed chain-like aggregates [78]. The particle size of iron nanoparticles also depends on the method of synthesis. The average size of iron nanoparticles ranging from 1 nm to 4 nm was synthesized by tunable synthesis for environmental applications [83]. TEM and high-resolution TEM images suggest a core nature of the particles containing of elemental iron covered with an oxide layer.

The superparamagnetic iron oxide nanoparticles [79] consisted of clusters of iron oxide monocrystals, embedded inside the polymer chains [79]. The TEM images showed the

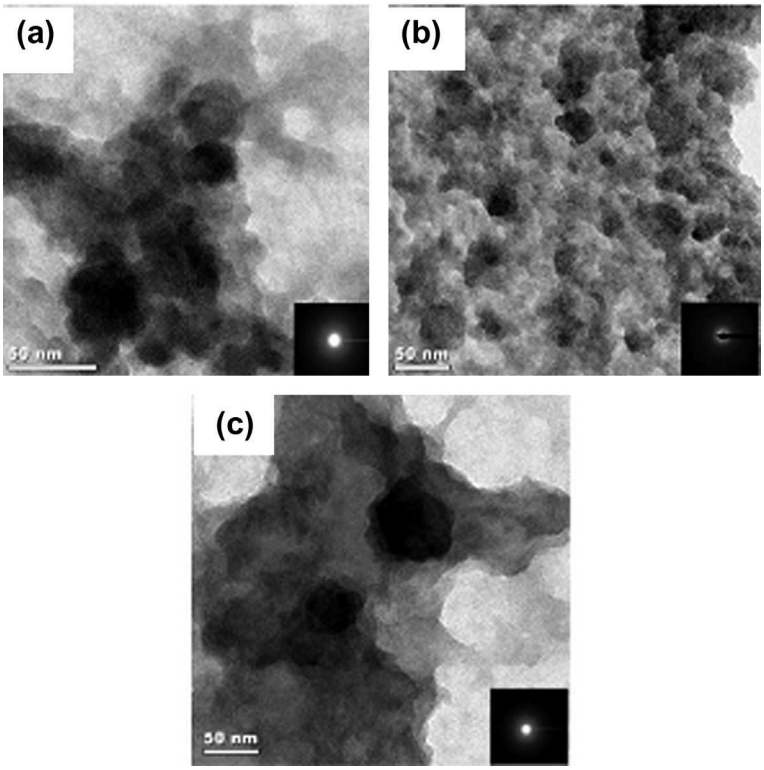

FIGURE 3.2 Representative TEM images of iron nanoparticles synthesized using sorghum bran extracts in water extracted at (a) 25 °C, (b) 50 °C, and (c) 80 °C. Reprinted with permission from Ref. [48]. Copyright (2011) American Chemical Society.

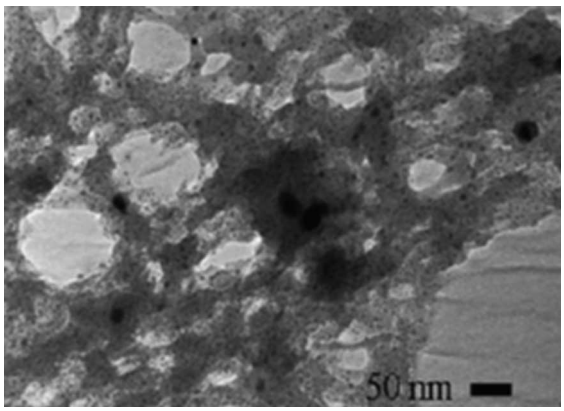

FIGURE 3.3 Representative TEM image of iron nanomaterial synthesized using a tea extract. Reproduced from Ref. [27] with permission from The Royal Society of Chemistry.

particles consisted of clusters of a few small iron oxide dots and each individual dot (monocrystalline iron oxide particles) was about 10 nm in diameter. In another study, TEM micrographs of prepared magnetic iron oxide nanoparticles revealed the spherical shape of the particles [80]. Au-coated iron nanoparticles were prepared by Ban et al. in which the iron core of the particle was covered by a shell of gold [81]. TEM images of the particles showed the dark contrast on the central part of Fe with a size of about 11 nm covered by a light contrast 2.5 nm shell of Au.

3.2.3 Textural and Surface Properties

The surface area and pore characteristics of iron nanoparticles play an important role in their catalytic activities. The classical BET (the Brunauer-Emmett-Teller isotherm) method is used to provide this information for a particular nanomaterial. The BET surface areas of zero-valent iron nanoparticles were found to be an average of $14.5\,m^2\,kg^{-1}$ [78]. The metallic iron nanoparticles prepared by Nurmi et al. using the geolith synthesis method, Fe^{H2} were found to have an average specific surface area from TEM images with of about $25\,m^2\,g^{-1}$, assuming the particles are spherical [82].

X-ray photoelectron spectroscopy (XPS) provides surface analysis of the particles. The XPS spectra for GT-Fe NPs gives the same information about the surface elements as EDX data [55]. The photoelectron profile of Fe 2p contains the characteristic $2p_{3/2}$ and $2p_{1/2}$ peaks at 711.5 eV and 725.2 eV, respectively. The energy corresponding to the first peak is typical for iron in iron oxide and in iron oxohydroxide.

3.2.4 Compositions

The composition of nanoparticles is mainly determined by energy-dispersive X-ray spectroscopy (EDX) analysis. Sometimes there might be some additional peaks in the EDX spectra which come from the precursors for the green-synthesized nanoparticles. In the EDXS spectra of green tea synthesized iron nanomaterials, the atomic percentage of different elements was 47.9% C, 6.3% O, 12.5% Na, 5.5% Cl, and 27.8% Fe [55]. The XPS data for iron nanomaterials prepared by Gao et al. along with the XRD patterns elucidated the compositions of the particles [77]. The binding energies corresponding to $Fe2p_{3/2}$, $Fe2p_{1/2}$, and O1s transitions were 711 eV, 725 eV, and 531 eV, respectively, which were all correlated to Fe_3O_4 material. In the study by Njagi et al. the EDXS spectrum revealed that the iron nanoparticles were mainly composed of iron with very little chlorine and phosphorus impurities [48]. The composition of Au-coated iron nanoparticles was estimated by EDXS [81]. EDXS showed the presence of iron and gold in the nanoparticles.

3.3 APPLICATIONS

3.3.1 Organic Dyes

One of the important applications of nanotechnology is the use of nanomaterials as catalysts for environmental remediation [17–20]. For example, green-synthesized iron nanoparticles

are increasingly being utilized in environmental remediation and hazardous waste treatment [41]. Iron nanomaterials are very efficient in removing organic and inorganic contaminants in water due to their high surface areas, surface reactivities, and sorption capacities [17,51]. Dyes are a popular group of organic pollutants in water for which iron nanomaterials are being used as catalysts for degradation. Dyes are the major pollutants in textile wastewater industries. Synthetic dyes are generally toxic and mutagenic to living organisms in the aquatic environment [18]. We summarized in this section some of the applications of green-synthesized iron nanomaterials for organic dye degradation.

The reactivity of iron nanomaterials synthesized at room temperature using aqueous sorghum bran extracts was tested by the peroxide-catalyzed degradation of 500 mg L^{-1} bromothymol blue in water [48]. The degradation of bromothymol blue (BTB) occurred in the presence of H_2O_2 and iron nanoparticles, suggesting that the degradation occurred via a free-radical pathway. The degradation of BTB was fastest in the presence of 2% H_2O_2 and 0.66 mM iron nanoparticles leading to a 90% reduction in the concentration of BTB within 30 min. Results indicated that higher iron concentrations accelerated the degradation of the dye.

Hybrid photoactive iron-containing material (Fe_2O_3 and Fe_3C) from municipal sludge was used for the photocatalytic degradation of methylene blue dye [40]. The photoactivity of TiO_2-hydrid material as compared to neat TiO_2 (commercial) was up to one order magnitude higher, suggesting that iron phases in the hybrid material photoassisted the TiO_2 in the effective photodegradation of methylene blue dye. The iron oxide species played an important role in the photocatalytic behavior of the hybrid material. The mechanism involved the transfer of electron density from oxygen atoms to iron atoms under visible light irradiation, leading to a photochemical response. In a previous study, the Fenton and photo-Fenton processes for methylene blue dye were found to follow pseudo first-order kinetics achieving 100% total organic carbon reduction after 60 min and 30 min treatment, respectively [42].

A green, single-step synthesis of iron nanoparticles was conducted using tea (*Camellia sinensis*) polyphenols without the addition of any surfactant/polymers as capping or reducing agents [27]. The effect of iron-catalyzed H_2O_2 on the degradation of organic contaminant was examined using BTB (at pH 6) as a model water contaminant. The activity of iron nanoparticles was compared with those of iron-ethylenediamine tetraacetate and iron-(*S*,*S*)-ethylenediamine-*N*,*N*′-disuccinic acid as catalysts for free-radical production from H_2O_2. Results showed that the highest rate of BTB degradation occurred with nano zero-valent iron from green tea. The iron nanoparticles increased the catalysis of H_2O_2 and therefore increased the overall rate of the degradation of BTB.

Iron nanoparticles were similarly prepared using extracts of green tea leaves [55]. The iron nanomaterial contained mainly iron oxide and iron oxohydroxide, which was utilized as a Fenton-like catalyst for the decolorization of aqueous solutions containing methylene blue and methyl orange dyes. The results indicated a fast removal of the dyes with the kinetic data of methylene blue following a second-order removal rate, whereas those of methyl orange were closer to a first-order removal rate. The loading experiments indicated almost complete removal of both dyes from water over a wide range of concentrations (10–200 mg L^{-1}). The iron nanoparticles from green tea extracts demonstrated a more effective capability as a Fenton-like catalyst, both in terms of kinetics and percentage dye removal, as compared to iron nanoparticles produced via the borohydride reduction.

Zero-valent iron nanoparticles have been immobilized into electrospun polymer nanofibrous mats [67]. Electrospun poly(acrylic acid)/poly(vinyl alcohol) nanofibrous mats were treated at an elevated temperature to render them water stable. The produced composite nanofibrous mats exhibited a superior capability to decolorize acid fuchsine dye solution (a typical dye present in wastewater of printing and dyeing industry). The small and uniformly distributed iron nanoparticles were the properties of iron nanoparticles which favored reactive degradation of the dye. Findings from this study also suggested potential use of electrospun nanofibers as nanoreactors to synthesize reactive iron nanoparticles for a broad range of water remediation applications.

The degradation of Acid Orange 7 (AO7) dye was investigated using zero-valent iron/granular activated carbon in the absence and presence of ultrasound [36]. AO7 dye was chosen as a model of the water-soluble phenylazonaphthol dyes due to its wide application and resistance to biodegradation. The dye degradation efficiency by zero-valent iron/granular activated carbon was dramatically enhanced by ultrasound irradiation. The effects of zero-valent iron/granular activated carbon ratios and initial pH values on degradation rates were also studied. The suitable zero-valent iron/granular activated carbon ratio for the degradation of AO7 in the presence of ultrasound was 1:1 (v/v). The degradation was highly dependent on pH, and a decrease of the initial pH values from 12.0 to 4.0 led to an increase of degradation efficiencies. Sulfanilamide was the main residual degradation product in the solution.

Preferential and enhanced adsorption of the dyes containing hydroxyl (−OH) groups on iron oxide nanoparticles were investigated [53]. The –OH groups of Erichrome Black-T, Bromophenol Blue, Bromocresol Green, and Fluorescein dyes were adsorbed more strongly on the iron oxide surface as compared to Methyl Red, Methylene Blue, and Methyl Orange dyes, which do not have any −OH groups. The adsorption process was studied by varying different parameters (initial dye and iron oxide concentrations, pH) and evaluated in terms of kinetic and isotherm models. At high pH, the adsorbed dyes could be desorbed from the surface of iron nanoparticles.

3.3.2 Halogenated Compounds

3.3.2.1 Decabromodiphenyl Ether

Decabromodiphenyl ether (BDE 209) belongs to a class of widely used brominated flame retardants that are persistent in the environment [84]. While biotic and abiotic processes can degrade the contaminant in the environment, these processes produce less brominated congeners which are more toxic, more persistent, and more bioavailable than the parent compound [84–86]. nZVI is a powerful reducing agent and has been shown to be effective for the degradation of BDE 209.

Yu et al. compared the reactivity of conventionally prepared nanoscale versus subnanoscale ZVI toward the reduction of BDE 209. The conventional preparation involved dropwise addition of sodium borohydride solution to iron (III) chloride [101]. The subnanoscale particles were prepared using smectite clay as a template following the procedure by Gu et al. [87]. The clay was mixed with iron (III) chloride at pH 4 for 6 h then centrifuged to remove the supernatant. The sub-nanoscale particles of 0.5 nm in size debrominated the contaminant 10 times faster than those prepared by conventional methods (40 nm). The higher reactivity was attributed to smaller clusters of nZVI and the mechanism was noted to be a stepwise

debromination with less brominated products (di, tri, and tetra) forming at neutral pH, whereas pentabromodiphenyl ethers formed at pH 9.6.

Li et al. proposed the mechanism for the debromination of BDE 209 as a stepwise debromination, which followed first-order kinetics [100]. The nZVI was immobilized on a cation-exchange resin and the BDE 209 was completely degraded after 8 h. Dechlorination of decachloro biphenyl was also conducted but the rate was slower than the rate for the debromination of BDE 209.

The degradation of BDE 209 by nZVI at different pH values was investigated. The nanoparticles removed 90% of the contaminant in 40 min whereas microscale ZVI took 40 d in spite of using 40 times more of the catalyst [88]. The reaction rate was faster when the initial pH value was reduced from 10 to 5 and the reaction was found to be pseudo first order with respect to the contaminant concentration. Debromination from para positions was more difficult than from meta or ortho. Apart from the debromination process, adsorption was also noted to be responsible for removal of the parent compound.

Doping iron with a second metal to form a bimetallic particle for the degradation of BDE 209 has been investigated and found to be better than using iron alone. The nZVI palladized and non-palladized forms were used to degrade polybrominated diphenyl ethers [84]. A 0.3% Pd by weight was found to be the optimum amount of loading. The synthesized particles showed slower degradation as compared to commercial ones. In 1 wk, the unpalladized commercial N25 degraded BDE 209 to dibrominated, monobrominated and diphenyl ether (DE) as end products, whereas the palladized forms degraded the compound to mainly DE. Contrary to those found by Shih and Tai, the debromination of BDE 209 using the palladized iron nanoparticles showed preferential removal of para bromine. The removal of para bromines was remarkable since the catalyst potentially reduces the estrogenic potency of PBDE intermediates.

Fe-Ni bimetallic particles have also been investigated for the degradation of BDE 209. The effective degradation followed a *pseudo* first-order degradation with the rate of reaction increasing with particle amount, Ni/Fe ratio, and decreasing initial concentration of compound [16]. A stepwise hydrogen reduction was the main mechanism for the degradation. A disadvantage of using these particles was the Ni leaching of up to 14.83 mg L^{-1}.

When Fe–Ag nanoparticles were used in conjunction with microwave energy, a 97% of BDE 209 and a 78% of 2,2′,4,4′-tetrabromodiphenyl ether (BDE 47) degradation were obtained in 8 min [90]. The rate of degradation and the dehalogenation efficiency were improved as compared to using iron nanoparticles alone or using conventional heating. For BDE 209, di- to nonabrominated congeners formed, whereas for BDE 47, triphenyl ether to tri BDES were found. A stepwise dehalogenation with a sequential H substitution was the suggested mechanism for the debromination.

3.3.2.2 Other Brominated compounds

Other brominated compounds also showed effective degradation with nZVI or bimetallic iron nanomaterials. The degradation of three compounds namely, carbon tetrabromide, bromoform, and dibromomethane with Fe and Ni/Fe nanomaterials was investigated [91]. Ni/Fe nanomaterial was most reactive for dehalogenating the compounds. The main mechanism for dehalogenation of carbon tetrabromide and bromoform was hydrogenolysis. Seventy-six percent of dibromomethane degraded following a concerted reductive debromination mechanism to methane.

Tetrabromobisphenol A (TBBPA) was debrominated using Fe/Ag nanomaterials coupled with ultrasonic radiation [89]. TBBPA was completely degraded in 20 min using 1% wt. Ag loading and at pH 6 ± 0.5 and 30 °C. The bimetallic nanomaterials were better than nZVI in degrading the TBBPA. The major intermediates obtained were tri-, di-, and mono-BBPA. The mechanism proposed was the Ag-catalyzed formation of H atoms on the surface of the particles. These H atoms can replace Br in the C–Br bond, which can break with the use of high surface area Fe/Ag nanomaterials.

3.3.2.3 Tricholoroethene (TCE)

He and Zhao investigated the dechlorination of tricholoroethene (TCE) and found that water-soluble starch stabilized Fe–Pd bimetallic nanoparticles removed 98% of TCE in 1 h [24]. In the first 20 min, 1,1-dichloroethene (DCE) was formed. The palladized iron nanomaterials were shown to age with time and therefore lose their reactivity. The structural evolution of Pd–Fe nanoparticles was investigated and when exposed to water, the particles changed structure [68]. Within 24 h, no metallic iron was present as the Pd was already buried in an iron oxide matrix. The aged bimetallic nanoparticles showed 80% reduced dechlorination rate for TCE compared to fresh particles. Fe/Pd nanoparticles synthesized using sodium carboxy methyl cellulose as stabilizers have also been shown to effectively dechlorinate TCE [92]. The as-synthesized particles degraded TCE 17 times faster than the unstabilized ones following a pseudo first-order rate constant. The nanoparticles were also readily transported in a loamy-sand soil column and could be completely removed with three-bed volumes of DI water. Thus, these nanomaterials are potential candidates for field applications.

3.3.2.4 Other Chlorinated Compounds

The degradation of polychlorinated biphenyl (PCB) has been investigated by various researchers using various iron and iron bimetallic nanomaterials. When Fe/Pd bimetallic nanomaterials were impregnated onto a mesoporous granular activated carbon, PCBs were adsorbed on the surface of carbon and subsequently dechlorinated by the bimetallic nanoparticles [93]. The system was able to dechlorinate 2-chlorobiphenyl by 90% after 2 d. The remaining 10% was adsorbed on the activated carbon together with the biphenyl dechlorination product. Similarly, Fe–Pd bimetallic nanoparticles stabilized by a water-soluble starch were able to remove over 80% of PCB in less than 100 h, whereas the unstarched particles removed only 24% of PCB [24]. Using nZVI immobilized on a cation-exchange resin, the dechlorination of decachlorobiphenyl was successfully achieved after 10 d (Li et al., 2007). However, when particles were suspended in solution for the same duration, 21% of the parent compound remained.

nZVI was used to reduce eight chlorinated ethanes [102]. Most ethane molecules were dechlorinated, except 1,2-dichloroethane. The reactivity of the nZVI was dependent on the degree of chlorination and the location of chlorine atoms on the molecule. A higher rate of dechlorination was observed with highly chlorinated ethanes and when the chlorine atoms were localized on a single carbon atom. Dechlorination of hexachloroethane was most efficient and followed a reductive β-elimination (two chlorine atoms from adjacent carbons were removed followed by double bond formation) pathway forming PCE (tetrachloroethylene) as the major product.

Comparing biodegradation of monochloroethane with nZVI-assisted dechlorination of the compound, there was a significant difference in the degradation of the products formed [94]. The products of abiotic dichloro-elimination degraded 10% more than the products of biodegradation. This suggests that the degradation of chlorinated ethane by nZVI is superior to biodegradation since the products of the former degraded faster than those from the latter reaction.

Removal of 1,1,1,-trichloroethane using a series of bimetallic iron nanomaterials (Au, Cu, Ni, Pd, and Pt) did not show any periodic trend [95]. However, the first order rate constant for the reactions correlated with the solubility of atomic hydrogen on the second metal. This suggested that the enhanced activity of bimetallic iron nanomaterials was due to absorbed atomic hydrogen and not by galvanic corrosion processes.

Freshly prepared Pd/Fe nanoparticles were used to dechlorinate mono-, di-, and 1,2,4-trichlorobenzene [96]. Successful dechlorination to form benzene as the final product was achieved. The reaction followed a *pseudo* first-order kinetics with more chlorinated products having higher reaction rates than the less chlorinated compounds. Pd/Fe nanomaterial was active since the unpalladized iron showed very minimal reactivity. The aged bimetallic particles had less activity presumably due to the dislodgment of Pd and Pd encapsulation by the iron oxides formed during aging.

Further investigation on the dechlorination of trichlorobenzene by Pd/Fe particles revealed that the presence of surfactants influenced the reaction rate [97]. When the concentrations of surfactants were below the critical micelle concentration (CMC) values of cationic (cetyltrimethylammonium bromide), anionic (sodium dodecyl sulfate), and nonionic (nonylphenol ethoxylate and octylphenol polyethylene glycol ether) surfactants, the rate constants increased as compared to pure water. However, above the CMC values, the rate decreased. The presence of natural organic matter (NOM) also reduced the catalytic dechlorination of 1,2,4-trichloro benzene by the particles due to competition with NOM as a H_2 acceptor.

Other aromatic chlorinated compounds investigated are chlorophenols. Hydrodechlorination of 2,4-dichlorophenol by nano Pd/Fe bimetallic particles was investigated [98]. Phenol was found to be the major product; however, trace levels of 2-chlorophenol and 4-chlorophenol were also formed. Optimum conditions such as high Pd loading, higher reaction temperatures, and weak acid conditions favored the catalytic dechlorination of these compound.

Dror et al. deposited nZVI and cyanocobalamine on a diatomite matrix and used the composite to study the degradation of PCE and tribromoneopentyl alcohol [99]. The resulting material was superior than nZVI material since it prevents agglomeration making the surface area larger. Laboratory experiments showed rapid first-order decay of the contaminants containing the composite material, whereas the concentration in the control remained the same. In addition, various chlorinated compounds in well water were passed through a column containing the composite for 30 min. The concentrations of contaminants were reduced considerably but the degradation rate was slower for the less chlorinated compounds. Field experiments were also conducted and well water was made to pass through a 50 kg of the composite material in a column. Inlet contained significant amounts of TCE, PCE, *cis*-DCE, carbon tetrachloride, and chloroform. These contaminants were reduced substantially in the outlet. Specifically, the concentrations of TCE and PCE were reduced to a third of inlet values. Other compounds degraded include nitrate ions and pesticides such as bromacyl and prometryn.

3.3.3 Non-Halogenated Compounds

The catalytic behavior of iron-based nanomaterials was investigated for the efficient decomposition of ethylene glycol and phenol through a Fenton-like reaction in the presence of H_2O_2 at room temperature, without the use of UV or visible radiation sources [72]. Complete oxygenation of ethylene glycol exhibited first-order reaction kinetics, whereas phenol decomposition may be simulated by an exponential decay. Complete mineralization was observed when sufficient amounts of catalyst and peroxide were used.

nZVI was also found to have high capacity for the removal and sequestration of malodorous sulfides such as hydrogen sulfide and dimethyl disulfide [33]. The core-shell structure of iron nanoparticles played a key role during the degradation reactions. Both iron in the core and FeOOH in the shell provided rich surface sites for the sorption of sulfides, whereas the surface-associated sulfide further reacted with hydrogen sulfide and evolved to iron polysulfide.

The degradation of hexahydro-1,3,5-trinitro-1,3,5-triazine (RDX) (a common contaminant of soil and water at military facilities) with zero-valent iron nanoparticles in water in the presence or absence of a stabilizer additive such as carboxymethyl cellulose or poly(acrylic acid) was also studied [46]. Results suggested that zero-valent iron nanoparticles degraded the RDX compound via an initial denitration and a sequential reduction to the corresponding nitroso derivatives prior to complete decomposition.nZVI materials were synthesized for pyrene removal from soil [11]. Batch experiments indicated that nZVI materials were more efficient in removing pyrene as compared to commercially available microscale zero-valent iron particles (<10 μm). Reaction kinetics of pyrene removal were dominated by the iron dosage and approximated by a *pseudo* first-order kinetics model. Results also indicated that the addition of nZVI produced strongly reducing conditions. Remediation of pyrene-contaminated soils is therefore a promising technology.

Novel and stable iron-supported catalysts were prepared by immobilizing Fe on commercial polyethylene via direct photo-Fenton attack with concomitant Fe deposition on the polyethylene surface [21]. Using this material, total degradation and a 50% resorcinol mineralization were observed in 40 min and 60 min, respectively, at an initial pH of 5.6 in the presence of H_2O_2. Homogeneous photo-Fenton reactions were responsible for the resorcinol degradation. The photocatalytic activity observed for the Fe/polymer film was dependent on the specific polymer capacity to release the initially deposited iron into the solution.

A simple and novel method to synthesize iron and aluminum-doped TiO_2 from wastewater was investigated and applied for the degradation of acetaldehyde [57]. A significant amount of acetaldehyde was removed with the use of Fe/TiO_2 and Al/TiO_2 nanomaterials under UV irradiation for 60 min. At higher Fe concentration, acetaldehyde removal decreased by ~50%. However, the photodecomposition of acetaldehyde using the Fe/TiO_2 and Al/TiO_2 was marginal under visible light irradiation.

3.4 CONCLUSIONS AND FUTURE DIRECTIONS

In this work, methods of iron-based nanomaterial synthesis and characterization have been reviewed. The literature suggests that during the last decade, a significant number of distinct methods have been developed for the preparation and material and process characterization

of nZVI, iron oxides, and other iron-containing nanomaterials. These methods include the traditional wet chemistry means, sophisticated modern synthesis techniques, and "green" methods using benign solvents and various plant extracts. The unique properties of materials at the nanoscale make them viable for industrial use as well. Iron nanomaterials have advantages over regular iron-based materials for both *in situ* and *ex situ* environmental engineering applications due to their high efficiency in the removal or reduction of contaminants. The nZVI can catalyze degradation of organic solvents in water more effectively when they are combined with emulsion liquid membranes. Iron-containing nanoparticles have also been applied in free and supported forms to achieve considerable levels of decontamination the result of their relatively low toxicity. Moreover, it is possible to tailor the activity and stability of iron nanoparticles by modifying their structural support. Iron nanoparticles generated using polyphenols are generally active catalysts, stable, easy to handle, and regenerable. There are various opportunities for industrial manufacturers to design their production processes in ways that can minimize adverse environmental impacts.

Various applications of iron nanomaterials in the field of environmental sciences and engineering have also been explored. The use of iron nanomaterials for remediation of organic pollutants in water bodies can be considered as a hot topic in the field of nanotechnology. The combination of a mixture of plant extracts and iron or iron and natural surfactants further assists or enhances the physical, chemical, and biological pollutant reduction processes. There are several benefits of the aforementioned approach: biodegradable and materials from natural sources are used; hazardous wastes are not produced; reduced processing is required; and materials produced are more stable and less prone to degradation. For example, iron nanoparticles can be produced using various plant extracts and agricultural materials such as sorghum bran, which can be used for catalytic activation of H_2O_2 and destruction of contaminated soils. A green chemistry approach is followed that not only produces nZVI with desired properties using benign solvents such as water, but also coats the iron nanoparticles to make the metal stable and active. Another example is the use of a green tea extract, which acts as both a reducing and a capping agent. This green chemistry approach is extended to membrane containing reactive nanoparticles (Fe and Fe/Pd) immobilized in a polymer film. Such membrane-supported bimetallic nanoparticles have found use in the dechlorination of TCE, an important environmental pollutant. At large scales, TCE degradation can be performed in a convective mode using either a pump-and-treat approach or a batch mode, wherein the membrane-bearing iron nanoparticles are injected underground. In summary, nZVI nanomaterial technology should become an increasingly popular choice for treatment of hazardous and toxic wastes, and for remediation of contaminated sites.

Although the preparation and characterization procedures of green-synthesized iron nanomaterials have almost been established, the mechanisms involving the interaction of these iron nanomaterials and the organic contaminants especially in complex aqueous phase (e.g., soil, groundwater, water, and wastewater) are still unclear. Therefore, further research in the form of actual testing/experimentation is necessary before widespread acceptance and adoption of iron nanomaterials is realized in environmental treatment processes. The kinetics involving iron nanomaterials needs to be studied for further understanding of the interaction of these nanoscale catalysts, oxidants, and substrates. Adequate delivery and transport models of iron nanomaterials in soil and groundwater need to be developed as they are critical to engineering applications. Future studies are needed to evaluate the potential adverse impacts

these iron nanomaterials could have on the environment outside of the active remediation zone. The lifetime of iron nanomaterials introduced the environment will continue to be a significant issue requiring further research. Instrumentation and analytical measurement techniques need to be developed in order to monitor and evaluate or predict how far iron nanomaterials can travel and the likelihood of bioaccumulation. Along with the growth of nanotechnology, the potential short- and long-term effects on human health and the environment must be seriously considered. Similar to other common nanomaterials such as TiO_2 and Ag nanoparticles, evaluation of toxicity of the iron-containing nanomaterials should be the focus of additional research of continued research as the effects of nanoparticles in environmental systems remain the subject of much debate and controversy.

Overall, there is great potential for green synthesis methods of iron nanomaterials to reduce the cost of remediation and other types of environmental treatment processes and shorten the time it takes to clean up a contaminated site, and enhance the minimization or complete elimination of contaminants in the environment. In order to prevent any adverse environmental impacts, it is our recommendation that additional evaluation of the fate, transport, reactivity, and toxicity of iron nanomaterials in environmental systems be studied prior during their use in sensitive ecosystems and applications or where human toxicity or ecotoxicity are major concerns. Key issues related to fate and transport, toxicity, and potential environmental impacts should continue to be studied. Laboratory and field methods for the sampling and analysis of nanomaterials in both natural environmental systems, as well as in engineered and remediation process, is in its infancy and should be focus of major research funding by both pubic and private sources. Nevertheless, green nanotechnologies will play pivotal roles in efforts to develop better methods to effectively detect and improve oxidative catalysis and reductant processes to treat harmful organic pollutants in the environment.

Acknowledgment

The authors gratefully acknowledge Dr. Dambar B. Hamal from the Department of Chemistry, University of Connecticut for his comments and suggestions.

References

[1] M. Ahmadi, F. Mashhoon, R. Kaveh, F. Tarkian, Use of mechanically prepared iron nano particles for nitrate removal from water, Asian J. Chem. 23 (3) (2011) 1205–1208.
[2] L. Alidokht, A.R. Khataee, A. Reyhanitabar, S. Oustan, Reductive removal of Cr(VI) by starch-stabilized Fe0 nanoparticles in aqueous solution, Desalination 270 (1–3) (2011) 105–110.
[3] S.A. Aromal, D. Philip, Green synthesis of gold nanoparticles using Trigonella foenum-graecum and its size-dependent catalytic activity, Spectrochim. Acta—Part A: Mol. Biomol. Spectrosc. 97 (2012) 1–5.
[4] S. Benmokhtar, H. Belmal, A.E. Jazouli, J.P. Chaminade, P. Gravereau, S. Pechev, J.C. Grenier, G. Villeneuve, D.D. Waal, Synthesis, structure, and physicochemical investigations of the new $FeCu_{0.50}TiO(PO_4)$ oxyphosphate, J. Solid State Chem. 180 (2) (2007) 772–779.
[5] A. Bharde, D. Rautaray, V. Bansal, A. Ahmad, I. Sarkar, S.M. Yusuf, M. Sanyal, M. Sastry, Extracellular biosynthesis of magnetite using fungi, Small 2 (1) (2006) 135–141.
[6] A. Bharde, A. Wani, Y. Shouche, P.A. Joy, B.L.V. Prasad, M. Sastry, Bacterial aerobic synthesis of nanocrystalline magnetite, J. Am. Chem. Soc. 127 (26) (2005) 9326–9327.
[7] A.A. Bharde, R.Y. Parikh, M. Baidakova, S. Jouen, B. Hannoyer, T. Enoki, B.L.V. Prasad, Y.S. Shouche, S. Ogale, M. Sastry, Bacteria-mediated precursor-dependent biosynthesis of superparamagnetic iron oxide and iron sulfide nanoparticles, Langmuir 24 (11) (2008) 5787–5794.

[8] M. Cao, Z. Li, J. Wang, W. Ge, T. Yue, R. Li, V.L. Colvin, W.W. Yu, Food related applications of magnetic iron oxide nanoparticles: enzyme immobilization, protein purification, and food analysis, Trends Food Sci. Technol. 27 (1) (2012) 47–56.
[9] P. Chandrasekaran, G. Viruthagiri, N. Srinivasan, The effect of various capping agents on the surface modifications of sol-gel synthesised ZnO nanoparticles, J. Alloy. Compd. 540 (2012) 89–93.
[10] H. Chang, C. Chang, H. Wu, Z. Guo, M. Yang, Y. Chiang, H. Sheu, N. Wu, Kinetic study on low-temperature synthesis of $LiFePO_4$ via solid-state reaction, J. Power Sources 158 (1) (2006) 550–556.
[11] M.C. Chang, H.Y. Kang, Remediation of pyrene-contaminated soil by synthesized nanoscale zero-valent iron particles, J. Environ. Sci. Health—Part A Tox. Hazard. Subst. Environ. Eng. 44 (6) (2009) 576–582.
[12] J. Chen, Z. Xiu, G.V. Lowry, P.J.J. Alvarez, Effect of natural organic matter on toxicity and reactivity of nano-scale zero-valent iron, Water Res. 45 (5) (2011) 1995–2001.
[13] P.S. Chowdhury, P.R. Arya, K. Raha, Green synthesis of nanoscopic iron oxide particles: A potential oxidizer in nanoenergetics, Synth. React. Inorg., Met.-Org., Nano-Met. Chem. 37 (6) (2007) 447–451.
[14] G.S. Dhillon, S.K. Brar, S. Kaur, M. Verma, Green approach for nanoparticle biosynthesis by fungi: current trends and applications, Crit. Rev. Biotechnol. 32 (1) (2012) 49–73.
[15] D.P.E. Dickson, Nanostructured magnetism in living systems, J. Magn. Magn. Mater. 203 (1–3) (1999) 46–49.
[16] Z. Fang, X. Qiu, J. Chen, X. Qiu, Debromination of polybrominated diphenyl ethers by Ni/Fe bimetallic nanoparticles: influencing factors, kinetics, and mechanism, J. Hazard. Mater. 185 (2–3) (2011) 958–969.
[17] H.C. Genuino, H. Huang, E.C. Njagi, L. Stafford, S.L. Suib, A review of green synthesis of nanophase inorganic materials for green chemistry applications, Handbook of Green Chemistry, Wiley-VCH Verlag GmbH & Co. KGaA, 2012 p. 217.
[18] H.C. Genuino, S. Dharmarathna, E.C. Njagi, M.C. Mei, S.L. Suib, Gas-phase total oxidation of benzene, toluene, ethylbenzene, and xylenes using shape-selective manganese oxide and copper manganese oxide catalysts, J. Phys. Chem. C 116 (22) (2012) 12066–12078.
[19] H.C. Genuino, D.B. Hamal, Y. Fu, S.L. Suib, Synergetic effects of ultraviolet and microwave radiation for enhanced activity of TiO_2 nanoparticles in degrading organic dyes using a continuous-flow reactor, J. Phys. Chem. C 116 (26) (2012) 14040–14051.
[20] H.C. Genuino, E.C. Njagi, E.M. Benbow, G.E. Hoag, J.B. Collins, S.L. Suib, Enhancement of the photodegradation of N-nitrosodimethylamine in water using amorphous and platinum manganese oxide catalysts, J. Photochem. Photobiol. A: Chem. 217 (2–3) (2011) 284–292.
[21] L.F. González-Bahamón, F. Mazille, L.N. Benítez, C. Pulgarín, Photo-Fenton degradation of resorcinol mediated by catalysts based on iron species supported on polymers, J. Photochem. Photobiol. A: Chem. 217 (1) (2011) 201–206.
[22] M. Gui, V. Smuleac, L.E. Ormsbee, D.L. Sedlak, D. Bhattacharyya, Iron oxide nanoparticle synthesis in aqueous and membrane systems for oxidative degradation of trichloroethylene from water, J. Nanopart. Res. 14 (5) (2012).
[23] J. Guo, R. Wang, W.W. Tjiu, J. Pan, T. Liu, Synthesis of Fe nanoparticles@graphene composites for environmental applications, J. Hazard. Mater. 225–226 (2012) 63–73.
[24] F. He, D. Zhao, Preparation and characterization of a new class of starch-stabilized bimetallic nanoparticles for degradation of chlorinated hydrocarbons in water, Environ. Sci. Technol. 39 (9) (2005) 3314–3320.
[25] R. Herrera-Becerra, J.L. Rius, C. Zorrilla, Tannin biosynthesis of iron oxide nanoparticles, Appl. Phys. A Mater. Sci. Process. 100 (2) (2010) 453–459.
[26] R. Herrera-Becerra, C. Zorrilla, J.L. Rius, J.A. Ascencio, Electron microscopy characterization of biosynthesized iron oxide nanoparticles, Appl. Phys. A Mater. Sci. Process. 91 (2) (2008) 241–246.
[27] G.E. Hoag, J.B. Collins, J.L. Holcomb, J.R. Hoag, M.N. Nadagouda, R.S. Varma, Degradation of bromothymol blue by 'greener' nano-scale zero-valent iron synthesized using tea polyphenols, J. Mater. Chem. 19 (45) (2009) 8671–8677.
[28] S. Iravani, Green synthesis of metal nanoparticles using plants, Green Chem. 13 (10) (2011) 2638–2650.
[29] A. Kahoul, A. Hammouche, Electrochemical performances of $FePO_4$-positive active mass prepared through a new sol-gel method, Ionics 16 (2) (2010) 105–109.
[30] D. Karabelli, S. Ünal, T. Shahwan, A.E. Eroğlu, Preparation and characterization of alumina-supported iron nanoparticles and its application for the removal of aqueous Cu^{2+} ions, Chem. Eng. J. 168 (2) (2011) 979–984.
[31] G.K. Kouassi, Magnetic and gold-coated magnetic iron oxide nanoparticles as detection tools: Preparation, characterization, and biosensing applications, Curr. Nanosci. 7 (4) (2011) 510–523.

[32] C.-L. Lee, C.-J.G. Jou, Reduced degradation of chlorobenzene in cosolvent solution using nanoscale zerovalent iron with microwave irradiation, Environ. Eng. Sci. 28 (3) (2011) 191–195.
[33] C.-C. Li, Y.-S. Lin, Interactions between organic additives and active powders in water-based lithium iron phosphate electrode slurries, J. Power Sources 220 (2012) 413–421.
[34] S. Li, W. Yan, W.-X. Zhang, Solvent-free production of nanoscale zero-valent iron (nZVI) with precision milling, Green Chem. 11 (10) (2009) 1618–1626.
[35] H. Lien, W.-X. Zhang, Nanoscale Pd/Fe bimetallic particles: Catalytic effects of palladium on hydrodechlorination, Appl. Catal. B: Environ. 77 (1–2) (2007) 110–116.
[36] H. Liu, G. Li, J. Qu, H. Liu, Degradation of azo dye Acid Orange 7 in water by Fe^0/granular activated carbon system in the presence of ultrasound, J. Hazard. Mater. 144 (1–2) (2007) 180–186.
[37] T. Liu, Z. Wang, L. Zhao, X. Yang, Enhanced chitosan/Fe0-nanoparticles beads for hexavalent chromium removal from wastewater, Chem. Eng. J. 189–190 (2012) 196–202.
[38] D.R. Lovley, J.F. Stolz, G.L.N. Jr, E.J.P. Phillips, Anaerobic production of magnetite by a dissimilatory iron-reducing microorganism, Nature 330 (6145) (1987) 252–254.
[39] N. Marx, L. Croguennec, D. Carlier, L. Bourgeois, P. Kubiak, F.L. Cras, C. Delmas, Structural and electrochemical study of a new crystalline hydrated iron(iii) phosphate $FePO_4{\cdot}H_2O$ obtained from $LiFePO_4(OH)$ by ion exchange, Chem. Mater. 22 (5) (2010) 1854–1861.
[40] J. Matos, M. Rosales, A. García, C. Nieto-Delgado, J.R. Rangel-Mendez, Hybrid photoactive materials from municipal sewage sludge for the photocatalytic degradation of methylene blue, Green Chem. 13 (12) (2011) 3431–3439.
[41] N.D. Meeks, V. Smuleac, C. Stevens, D. Bhattacharyya, Iron-based nanoparticles for toxic organic degradation: Silica platform and green synthesis, Ind. Eng. Chem. Res. 51 (28) (2012) 9581–9590.
[42] D. Melgoza, A. Hernández-Ramírez, J.M. Peralta-Hernández, Comparative efficiencies of the decolourisation of Methylene Blue using Fenton's and photo-Fenton's reactions, Photochem. Photobiol. Sci. 8 (5) (2009) 596–599.
[43] M.N. Nadagouda, A.B. Castle, R.C. Murdock, S.M. Hussain, R.S. Varma, In vitro biocompatibility of nanoscale zerovalent iron particles (NZVI) synthesized using tea polyphenols, Green Chem. 12 (1) (2010) 114–122.
[44] M.N. Nadagouda, G. Hoag, J. Collins, R.S. Varma, Green synthesis of Au nanostructures at room temperature using biodegradable plant surfactants, Cryst. Growth Des. 9 (11) (2009) 4979–4983.
[45] V. Nagpal, A.D. Bokare, R.C. Chikate, C.V. Rode, K.M. Paknikar, Reductive dechlorination of Î³-hexachlorocyclohexane using Fe–Pd bimetallic nanoparticles, J. Hazard. Mater. 175 (1–3) (2010) 680–687.
[46] G. Naja, A. Halasz, S. Thiboutot, G. Ampleman, J. Hawari, Degradation of hexahydro-1,3,5-trinitro-1,3,5-triazine (RDX) using zerovalent iron nanoparticles, Environ. Sci. Technol. 42 (12) (2008) 4364–4370.
[47] K.B. Narayanan, N. Sakthivel, Biological synthesis of metal nanoparticles by microbes, Adv. Colloid Interface Sci. 156 (1–2) (2010) 1–13.
[48] E.C. Njagi, H. Huang, L. Stafford, H. Genuino, H.M. Galindo, J.B. Collins, G.E. Hoag, S.L. Suib, Biosynthesis of iron and silver nanoparticles at room temperature using aqueous sorghum bran extracts, Langmuir 27 (1) (2011) 264–271.
[49] H. Park, Y.-C. Lee, B.G. Choi, Y.S. Choi, J.-W. Yang, W.H. Hong, Green one-pot assembly of iron-based nanomaterials for the rational design of structure, Chem. Commun. 27 (2009) 4058–4060.
[50] R. Peltier, W.R. Siah, G.V.M. Williams, M.A. Brimble, R.D. Tilley, D.E. Williams, Novel phosphopeptides as surface-active agents in iron nanoparticle synthesis, Aust. J. Chem. 65 (6) (2012) 680–685.
[51] G. Qiu, H. Huang, H. Genuino, N. Opembe, L. Stafford, S. Dharmarathna, S.L. Suib, Microwave-assisted hydrothermal synthesis of nanosized α-Fe_2O_3 for catalysts and adsorbents, J. Phys. Chem. C 115 (40) (2011) 19626–19631.
[52] F. Rajabi, N. Karimi, M.R. Saidi, A. Primo, R.S. Varma, R. Luque, Unprecedented selective oxidation of styrene derivatives using a supported iron oxide nanocatalyst in aqueous medium, Adv. Synth. Catal. 354 (9) (2012) 1707–1711.
[53] B. Saha, S. Das, J. Saikia, G. Das, Preferential and enhanced adsorption of different dyes on iron oxide nanoparticles: a comparative study, J. Phys. Chem. C 115 (16) (2011) 8024–8033.
[54] S.N. Shah, N.F. Steinmetz, A.A.A. Aljabali, G.P. Lomonossoff, D.J. Evans, Environmentally benign synthesis of virus-templated, monodisperse, iron-platinum nanoparticles, Dalton Trans. 40 (2009) 8479–8480.
[55] T. Shahwan, S. Abu Sirriah, M. Nairat, E. Boyaci, A.E. Eroğlu, T.B. Scott, K.R. Hallam, Green synthesis of iron nanoparticles and their application as a Fenton-like catalyst for the degradation of aqueous cationic and anionic dyes, Chem. Eng. J. 172 (1) (2011) 258–266.

[56] R.K. Sharma, S. Gulati, S. Mehta, Preparation of gold nanoparticles using tea: a green chemistry experiment, J. Chem. Educ. 89 (10) (2012) 1316–1318.
[57] H.K. Shon, D.L. Cho, S.H. Na, J.B. Kim, H.-J. Park, J.-H. Kim, Development of a novel method to prepare Fe- and Al-doped TiO_2 from wastewater, J. Ind. Eng. Chem. 15 (4) (2009) 476–482.
[58] A.K. Singh, V. Viswanath, V.C. Janu, Synthesis, effect of capping agents, structural, optical and photoluminescence properties of ZnO nanoparticles, J. Lumin. 129 (8) (2009) 874–878.
[59] R. Singh, V. Misra, R.P. Singh, Removal of Cr(VI) by nanoscale zero-valent iron (nZVI) from soil contaminated with tannery wastes, Bull. environ. contamination toxicol. 88 (2) (2012) 210–214.
[60] R. Singh, A. Singh, V. Misra, R.P. Singh, Degradation of lindane contaminated soil using zero-valent iron nanoparticles, J. Biomed. Nanotechnol. 7 (1) (2011) 175–176.
[61] V. Smuleac, R. Varma, S. Sikdar, D. Bhattacharyya, Green synthesis of Fe and Fe/Pd bimetallic nanoparticles in membranes for reductive degradation of chlorinated organics, J. Membr. Sci. 379 (1–2) (2011) 131–137.
[62] S. Srivastava, R. Awasthi, N.S. Gajbhiye, V. Agarwal, A. Singh, A. Yadav, R.K. Gupta, Innovative synthesis of citrate-coated superparamagnetic Fe_3O_4 nanoparticles and its preliminary applications, J. Colloid Interface Sci. 359 (1) (2011) 104–111.
[63] Y. Sun, X. Li, W. Zhang, H.P. Wang, A method for the preparation of stable dispersion of zero-valent iron nanoparticles, Colloids Surf. A 308 (1–3) (2007) 60–66.
[64] Y. Tee, L. Bachas, D. Bhattacharyya, Degradation of trichloroethylene and dichlorobiphenyls by iron-based bimetallic nanoparticles, J. Phys. Chem. C 113 (22) (2009) 9454–9464.
[65] L. Tong, M. Zhao, S. Zhu, J. Chen, Synthesis and application of superparamagnetic iron oxide nanoparticles in targeted therapy and imaging of cancer, Front. Med. China 5 (4) (2011) 379–387.
[66] N. Vigneshwaran, N.M. Ashtaputre, P.V. Varadarajan, R.P. Nachane, K.M. Paralikar, R.H. Balasubramanya, Biological synthesis of silver nanoparticles using the fungus Aspergillus flavus, Mater. Lett. 61 (6) (2007) 1413–1418.
[67] S. Xiao, M. Shen, R. Guo, S. Wang, X. Shi, Immobilization of zerovalent iron nanoparticles into electrospun polymer nanofibers: synthesis, characterization, and potential environmental applications, J. Phys. Chem. C 113 (42) (2009) 18062–18068.
[68] W. Yan, A.A. Herzing, X. Li, C.J. Kiely, W. Zhang, Structural evolution of Pd doped nanoscale zero-valent iron (nZVI) in aqueous media and implications for particle aging and reactivity, Environ. Sci. Technol. 44 (11) (2010) 4288–4294.
[69] X. Yang, S.M. Zhang, J.X. Zhang, M.Y. Xu, P. Ren, X.C. Li, L.C. Yan, The study on synthesis and modification for iron phosphate, Funct. Mater. Lett. 4 (4) (2011) 323–326.
[70] Y. Yin, H. Zhang, P. Wu, B. Zhou, C. Cai, Iron phosphate nanostructures synthesized by microwave method and their applications in biosensing, Nanotechnology 21 (42) (2010).
[71] K. Zaghib, C.M. Julien, Structure and electrochemistry of $FePO_4{\cdot}2H_2O$ hydrate, J. Power Sources 142 (1–2) (2005) 279–284.
[72] G. Zelmanov, R. Semiat, Iron(3) oxide-based nanoparticles as catalysts in advanced organic aqueous oxidation, Water Res. 42 (1–2) (2008) 492–498.
[73] M. Zhang, F. He, D. Zhao, X. Hao, Degradation of soil-sorbed trichloroethylene by stabilized zero valent iron nanoparticles: effects of sorption, surfactants, and natural organic matter, Water Res. 45 (7) (2011) 2401–2414.
[74] W.X. Zhang, Nanoscale iron particles for environmental remediation: an overview, J. Nanopart. Res. 5 (3–4) (2003) 323–332.
[75] W. Zhou, W. He, X. Zhang, S. Yan, X. Sun, X. Tian, X. Han, Biosynthesis of iron phosphate nanopowders, Powder Technol. 194 (1–2) (2009) 106–108.
[76] N. Zhu, H. Luan, S. Yuan, J. Chen, X. Wu, L. Wang, Effective dechlorination of HCB by nanoscale Cu/Fe particles, J. Hazard. Mater. 176 (1–3) (2010) 1101–1105.
[77] S. Gao, Y. Shi, S. Zhang, K. Jiang, S. Yang, Z. Li, E. Takayama-Muromachi, Biopolymer-assisted green synthesis of iron oxide nanoparticles and their magnetic properties, J. Phys. Chem. C 112 (28) (2008) 10398–10401.
[78] Y. Sun, X. Li, J. Cao, W. Zhang, H.P. Wang, Characterization of zero-valent iron nanoparticles, Adv. Colloid Interface Sci. 120 (1–3) (2006) 47–56.
[79] S. Liu, X. Wei, M. Chu, J. Peng, Y. Xu, Synthesis and characterization of iron oxide/polymer composite nanoparticles with pendent functional groups, Colloids Surf. B 51 (2) (2006) 101–106.
[80] A.B. Chin, I.I. Yaacob, Synthesis and characterization of magnetic iron oxide nanoparticles via w/o microemulsion and Massart's procedure, J. Mater. Process. Technol. 191 (1–3) (2007) 235–237.

[81] Z. Ban, Y.A. Barnakov, F. Li, V.O. Golub, C.J. O'Connor, The synthesis of core-shell iron@gold nanoparticles and their characterization, J. Mater. Chem. 15 (43) (2005) 4660–4662.
[82] J.T. Nurmi, P.G. Tratnyek, V. Sarathy, D.R. Baer, J.E. Amonette, K. Pecher, C. Wang, J.C. Linehan, D.W. Matson, R.L. Penn, M.D. Driessen, Characterization properties of metallic iron nanoparticles: spectroscopy, electrochemistry, and kinetics, Environ. Sci. Technol. 39 (5) (2005) 1221–1230.
[83] Q. Huang, X. Shi, R.A. Pinto, E.J. Petersen, W.J. Weber Jr., Tunable synthesis and immobilization of zero-valent iron nanoparticles for environmental applications, Environ. Sci. Technol. 42 (33) (2008) 8884–8889.
[84] Y. Zhuang, L. Jin, R.G. Luthy, Kinetics and pathways for the debromination of polybrominated diphenyl ethers by bimetallic and nanoscale zerovalent iron: effects of particle properties and catalyst, Chemosphere 89 (4) (2012) 426–432.
[85] S. Ciparis, R.C. Hale, Bioavailability of polybrominated diphenyl ether flame retardants in biosolids and spiked sediment to the aquatic *Oligochaete*, *Lumbriculus variegates*, Environ. Toxicol. Chem. 24 (4) (2005) 916–925.
[86] J.A. Tokarz III, M. Ahn, J. Leng, T.R. Filley, L. Nies, Reductive debromination of polybrominated diphenyl ethers in anaerobic sediment and a biomimetic system, Environ. Sci. Technol. 42 (4) (2008) 1157–1164.
[87] C. Gu, H. Jia, H. Li, B.J. Teppen, S.A. Boyd, Synthesis of highly reactive subnano-sized zero-valent iron using smectite clay templates, Environ. Sci. Technol. 44 (11) (2010) 4258–4263.
[88] Y. Shih, Y. Tai, Reaction of decabrominated diphenyl ether by zerovalent iron nanoparticles, Chemosphere 78 (10) (2010) 1200–1206.
[89] S. Luo, S. Yang, X. Wang, C. Sun, Reductive degradation of tetrabromobisphenol A over iron-silver bimetallic nanoparticles under ultrasound radiation, Chemosphere 79 (6) (2010) 672–678.
[90] S. Luo, S. Yang, C. Sun, J. Gu, Improved debromination of polybrominated diphenyl ethers by bimetallic iron-silver nanoparticles coupled with microwave energy, Sci. Total Environ. 429 (2012) 300–308.
[91] T. Lim, J. Feng, B. Zhu, Kinetic and mechanistic examinations of reductive transformation pathways of brominated methanes with nano-scale Fe and Ni/Fe particles, Water Res. 41 (4) (2007) 875–883.
[92] F. He, D. Zhao, J. Liu, C.B. Roberts, Stabilization of Fe–Pd nanoparticles with sodium carboxymethyl cellulose for enhanced transport and dechlorination of trichloroethylene in soil and groundwater, Ind. Eng. Chem. Res. 46 (1) (2007) 29–34.
[93] H. Choi, S.R. Al-Abed, S. Agarwal, D.D. Dionysiou, Synthesis of reactive nano-Fe/Pd bimetallic system-impregnated activated carbon for the simultaneous adsorption and dechlorination of PCBs, Chem. Mater. 20 (11) (2008) 3649–3655.
[94] M. Elsner, M. Chartrand, N. Vanstone, G.L. Couloume, B.S. Lollar, Identifying abiotic chlorinated ethene degradation: characteristic isotope patterns in reaction products with nanoscale zero-valent iron, Environ. Sci. Technol. 42 (16) (2008) 5963–5970.
[95] D.M. Cwiertny, S.J. Bransfield, K.J.T. Livi, D.H. Fairbrother, A.L. Roberts, Exploring the influence of granular iron additives on 1,1,1-trichloroethane reduction, Environ. Sci. Technol. 40 (21) (2006) 6837–6843.
[96] B. Zhu, T. Lim, Catalytic reduction of chlorobenzenes with Pd/Fe nanoparticles: reactive sites, catalyst stability, particle aging, and regeneration, Environ. Sci. Technol. 41 (21) (2007) 7523–7529.
[97] B. Zhu, T. Lim, J. Feng, Influences of amphiphiles on dechlorination of a trichlorobenzene by nanoscale Pd/Fe: adsorption, reaction kinetics, and interfacial interactions, Environ. Sci. Technol. 42 (12) (2008) 4513–4519.
[98] J. Wei, X. Xu, Y. Liu, D. Wang, Catalytic hydrodechlorination of 2,4-dichlorophenol over nanoscale Pd/Fe: reaction pathway and some experimental parameters, Water Res. 40 (2) (2006) 348–354.
[99] I. Dror, O.M. Jacov, A. Cortis, B. Berkowitz, Catalytic transformation of persistent contaminants using a new composite material based on nanosized zero-valent iron, ACS Appl. Mater. Interfaces 4 (7) (2012) 3416–3423.
[100] A. Li, C. Tai, Z. Zhao, Y. Wang, Q. Zhang, G. Jiang, J. Hu, Debromination of decabrominated diphenyl ether by resin-bound iron nanoparticles, Environ. Sci. Technol. 41 (19) (2007) 6841–6846.
[101] K. Yu, C. Gu, S.A. Boyd, C. Liu, C. Sun, B.J. Teppen, H. Li, Rapid and extensive debromination of decabromodiphenyl ether by smectite clay-templated subnanoscale zero-valent iron, Environ. Sci. Technol. 46 (16) (2012) 8969–8975.
[102] H. Song, E.R. Carraway, Reduction of chlorinated ethanes by nanosized zero-valent iron: Kinetics, pathways, and effects of reaction conditions, Environ. Sci. Technol. 39 (16) (2005) 6237–6245.